

PAPER

# Dynamically tunable plasmon-induced transparency effect based on graphene metasurfaces

To cite this article: Shuxian Chen *et al* 2022 *J. Phys. D: Appl. Phys.* **55** 115105

View the [article online](#) for updates and enhancements.

## You may also like

- [Stress distribution and lattice distortions in Nb<sub>3</sub>Sn multifilament wires under uniaxial tensile loading at 4.2 K](#)  
C Scheuerlein, M Di Michiel, F Buta *et al.*
- [An ultrafast and low-power slow light tuning mechanism for compact aperture-coupled disk resonators](#)  
Bo-Yun Wang, , Yue-Hong Zhu *et al.*
- [Mechanical control of terahertz plasmon-induced transparency in single/double-layer stretchable metamaterial](#)  
Jing Wang, Hao Tian, Guanchao Wang *et al.*



**IOP | ebooks™**

Bringing together innovative digital publishing with leading authors from the global scientific community.

Start exploring the collection—download the first chapter of every title for free.

# Dynamically tunable plasmon-induced transparency effect based on graphene metasurfaces

Shuxian Chen<sup>1</sup> , Junyi Li<sup>1</sup>, Zicong Guo<sup>1</sup>, Li Chen<sup>1,3</sup> , Kunhua Wen<sup>1,3,\*</sup> , Pengbai Xu<sup>2,3</sup>, Jun Yang<sup>2,3</sup> and Yuwen Qin<sup>2,3</sup>

<sup>1</sup> School of Physics and Optoelectronic Engineering, Guangdong University of Technology, Guangzhou 510006, People's Republic of China

<sup>2</sup> School of Information Engineering, Guangdong University of Technology, Guangzhou 510006, People's Republic of China

<sup>3</sup> Guangdong Provincial Key Laboratory of Information Photonics Technology, Guangdong University of Technology, Guangzhou 510006, People's Republic of China

E-mail: [khwen@gdut.edu.cn](mailto:khwen@gdut.edu.cn)

Received 6 September 2021, revised 21 November 2021

Accepted for publication 2 December 2021

Published 16 December 2021



CrossMark

## Abstract

Plasmon-induced transparency (PIT) is theoretically explored for a graphene metamaterial using finite-difference time-domain numerical simulations and coupled-mode-theory theoretical analysis. In this work, the proposed structure consists of one rectangular cavity and three strips to generate the PIT phenomenon. The PIT window can be regulated dynamically by adjusting the Fermi level of the graphene. Importantly, the modulation depth of the amplitude can reach 90.4%. The refractive index sensitivity of the PIT window is also investigated, and the simulation results show that a sensitivity of  $1.335 \text{ THz RIU}^{-1}$  is achieved. Additionally, when the polarization angle of the incident light is changed gradually from  $0^\circ$  to  $90^\circ$ , the performance of the structure is greatly affected. Finally, the proposed structure is particularly enlightening for the design of dynamically tuned terahertz devices.

Keywords: graphene, plasmon-induced transparency, optical switch, high sensitivity, mode

(Some figures may appear in color only in the online journal)

## 1. Introduction

Surface plasmon polaritons (SPPs) are surface electromagnetic waves, that exist on the metal-dielectric interface. SPPs have received widespread attention for their capability for light confinement and breaking through the classical optical diffraction limit. However, in the traditional metal-dielectric structures, the materials are made of noble metals, such as silver and gold [1, 2]. These reported structures usually work in the near-infrared band, and the SPPs resonance must be statically adjusted by designing the geometric parameters.

Currently, graphene displays dynamic wavelength tuning characteristics in the terahertz band and has become a potential research platform for surface plasmons (SPs) [3]. There are two main advantages for graphene-based devices. First, the SP modes can be excited on the graphene material and propagate with negligible losses [4, 5]. In addition, the conductivity of graphene can be flexibly adjusted by changing the structure and gate voltage [6–9].

The plasmon-induced transparency (PIT) phenomenon, which is also generated with SPPs, possesses great controllability by adjusting graphene. The physical origin of the PIT is the destructive interference between the bright mode and the dark mode [10]. In general, the PIT gives rise to a sharp transparency window within a broad absorption spectrum. Interesting applications using the PIT have been developed,

\* Author to whom any correspondence should be addressed.

for example, the required wavelength shift can be provided by heating the structure, reflecting its potential in realizing compact switching components [11]. By taking advantage of the special phenomenon of PIT, many other nanophotonic devices have been proposed and demonstrated, such as optical switching [12, 13], optical absorbers [14], slow-light devices [15], sensing [16], etc.

The PIT effect of SPs is generally caused by the coupling of two resonators. In the traditional SP waveguide structure [17], a metal baffle can be added to the resonant cavity to change the resonant condition and improve the sensing performance. However, the regulated mode is static when using this approach.

In this paper, the PIT effect is achieved in the proposed periodic patterned graphene structure. The PIT transmission spectrum is obtained using the finite-difference time-domain (FDTD), where periodic boundary conditions are used for a unit cell in the  $x$ - and  $y$ -directions, and the  $z$ -directions have a perfectly matched layer boundary condition. The electric field distributions are used to explain the PIT phenomenon, and their transmission spectrum is fitted by the coupled mode theory (CMT). Interestingly, the on-off modulation gained by controlling the Fermi level of graphene is realized with the amplitude-modulation depth of 90.4%. In addition, the high sensitivity of refractive index corresponding to the peak of the structure is analyzed and investigated numerically. Moreover, the influence of the polarization angle of incident light on the PIT window is investigated. Consequently, the PIT can be produced by our graphene structure and dynamically regulated by the Fermi level. The size of the structure does not need to be changed so it is of great practical value.

## 2. Structural model and theoretical analysis

The schematic diagram of the graphene-metamaterial structure is shown in figure 1(a), and the corresponding top view is shown in figure 1(b). There is a corresponding relationship between the frequency and the structure. The wave vector of SP satisfies the conditions of  $k_{\text{spp}} \propto 1/L$  and  $k_{\text{spp}} = \hbar\omega_r^2 / (2\alpha_0 E_{\text{FC}}) = 2\pi^2 \hbar c / (\alpha_0 E_{\text{F}} \lambda_r^2)$  [18], where  $L$  is the length of the graphene nanostrip,  $\alpha_0 = e^2 / (\hbar c)$  is the fine structure constant, and  $\lambda_r$  is the resonant wavelength. Thus, the PIT resonance frequency is related to the geometrical parameters, which are calculated and optimized through the resonance formula. The geometric parameters in figure 1(b) are as follows:  $L = 4 \mu\text{m}$ ,  $S_1 = 2.1 \mu\text{m}$ ,  $S_2 = 2.7 \mu\text{m}$ ,  $S_3 = 3.25 \mu\text{m}$ ,  $S_4 = 0.8 \mu\text{m}$ ,  $S_5 = 0.25 \mu\text{m}$ ,  $S_6 = 0.3 \mu\text{m}$ ,  $S_7 = 0.3 \mu\text{m}$ ,  $S_8 = 0.4 \mu\text{m}$ ,  $S_9 = 0.2 \mu\text{m}$ ,  $S_{10} = 0.15 \mu\text{m}$ . The substrate is silica, of which the advantage is to prevent the oxidation reaction of the structure and improve the stability of the structure. The substrate thickness is set as  $0.2 \mu\text{m}$ . The silica is assumed to be lossless with the constant refractive index of  $n_{\text{SiO}_2} = 1.45$  [19].

In the calculations, the periodical boundary conditions are used in the  $x$ - and  $y$ -directions, and the perfectly matched layer is employed in the  $z$ -direction. Additionally, the mesh sizes in the proposed system and the simulation time are set to

$0.1 \mu\text{m}$  and  $15\,000 \text{ fs}$ , respectively, and the light source is a  $x$ -polarized planar wave in the negative direction of the  $z$  axis, respectively.

From the Kubo formula, the conductivity of graphene includes the interband and intraband contributions, and is expressed as follows [20–23]:

$$\left\{ \begin{aligned} \sigma(\omega, E_{\text{f}}, \tau, T) &= \frac{e^2(\omega + i\tau^{-1})}{i\pi\hbar^2} \\ &\times \left[ \frac{1}{(\omega + i\tau^{-1})^2} \int_0^{+\infty} \varepsilon \left( \frac{\partial f_{\text{d}}(\varepsilon)}{\partial \varepsilon} - \frac{\partial f_{\text{d}}(-\varepsilon)}{\partial \varepsilon} \right) d\varepsilon \right] \\ &- \int_0^{+\infty} \varepsilon \left( \frac{f_{\text{d}}(-\varepsilon) - f_{\text{d}}(\varepsilon)}{(\omega + i\tau^{-1})^2 - 4(\varepsilon/\hbar)^2} d\varepsilon \right) = \sigma^{\text{intra}} + \sigma^{\text{inter}}, \\ \sigma^{\text{intra}} &= \frac{2ie^2 k_{\text{B}} T}{\pi\hbar^2(\omega + i\tau^{-1})} \ln \left[ 2 \cosh \left( \frac{E_{\text{f}}}{2k_{\text{B}} T} \right) \right], \\ \sigma^{\text{inter}} &= \frac{ie^2(\omega + i\tau^{-1})}{4\pi k_{\text{B}} T} \int_0^{+\infty} \frac{G(\zeta)}{h(\omega + i\tau^{-1})^2 / (2k_{\text{B}} T)^2 - \zeta^2} d\zeta, \end{aligned} \right. \quad (1)$$

$$G(\zeta) = \frac{\sinh \zeta}{\cosh \frac{E_{\text{f}}}{k_{\text{B}} T} + \cosh \zeta}, \zeta = \frac{\varepsilon}{k_{\text{B}} T}, \quad (2)$$

where  $\omega$  is the angle frequency of incident light and  $\tau$  is the carrier relaxation time.  $\tau$  is calculated from  $\tau = (\mu E_{\text{f}}) / (e v_{\text{F}}^2)$  and depends on the carrier mobility  $\mu$ .  $\mu$  is set to  $10\,000 \text{ cm}^2 \text{V s}^{-1}$  and  $v_{\text{F}}$  is set to  $1 \times 10^6 \text{ m s}^{-1}$ .  $\varepsilon$  is the dielectric of graphene,  $k_{\text{B}}$  is the Boltzmann constant.  $T$  is the environment temperature with a constant value of  $300 \text{ K}$ . Here,  $f_{\text{d}}(\varepsilon)$  is Fermi–Dirac distribution, in which,  $f_{\text{d}}(\varepsilon) = 1 / [1 + e^{(\varepsilon - E_{\text{f}}) / (k_{\text{B}} T)}]$ .

The optical modulation frequency is set in the terahertz region with the Fermi level  $E_{\text{f}} \gg k_{\text{B}} T$  [23]. Therefore, under these parameters, the interband contributions  $\sigma^{\text{inter}}$  can be neglected, and the conductivity can be fully contributed by the intraband contributions  $\sigma^{\text{intra}}$ . Consequently, from equation (1), we can further obtain a simple expression of the conductivity,

$$\begin{aligned} \sigma &\approx \sigma^{\text{intra}} \approx \frac{2ie^2 k_{\text{B}} T}{\pi\hbar^2(\omega + i\tau^{-1})} \ln \left[ \exp \left( \frac{E_{\text{f}}}{2k_{\text{B}} T} \right) \right] \\ &= \frac{ie^2 E_{\text{f}}}{\pi\hbar^2(\omega + i\tau^{-1})}. \end{aligned} \quad (3)$$

The propagation constant of graphene is obtained by [24, 25]:

$$\beta = k_0 \sqrt{\varepsilon_{\text{r}} - \left( \frac{2\varepsilon_{\text{r}}}{\sigma\eta_0} \right)^2} \quad (4)$$

where  $\sigma$  represents the complex conductivity of graphene,  $\varepsilon_{\text{r}}$  is the relative permittivity of silica.  $k_0$  and  $\eta_0$  correspond to the wavenumber of the traveling wave and the intrinsic impedance in the free space, respectively.

Regarding the CMT theory [26–28], the bright and dark modes in the structure correspond to  $B$  and  $D$ , and the composite amplitudes are denoted by  $b$  and  $d$ , as shown in figure 2.

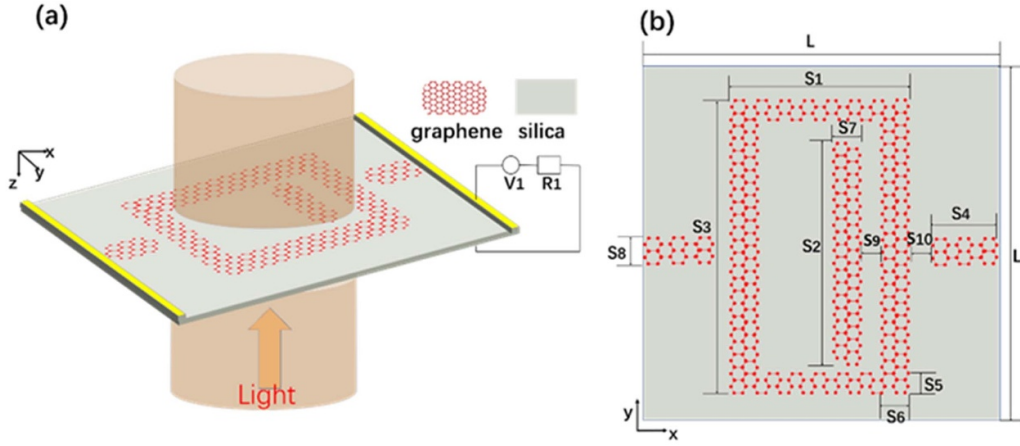


**Figure 1.** (a) Structure unit of the proposed periodic metamaterial. (b) Top view of the structure.

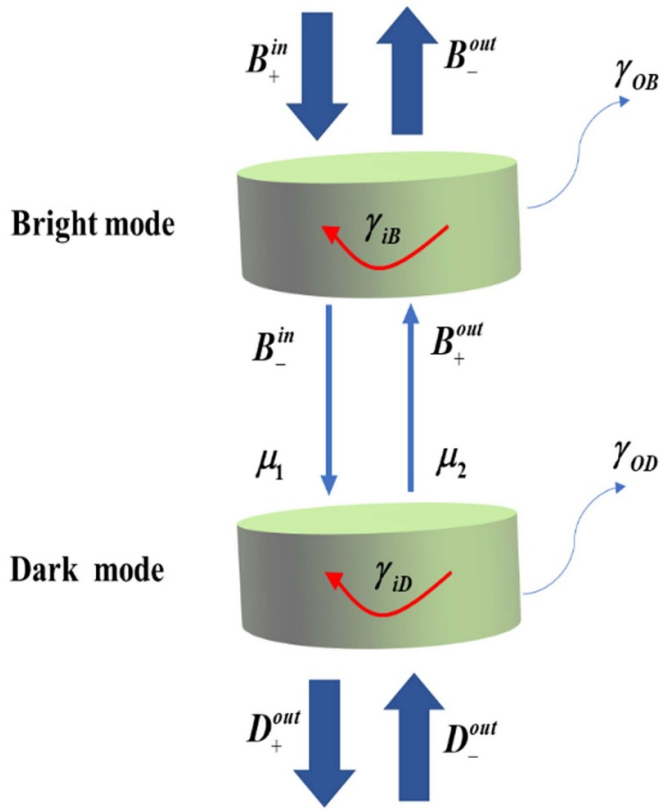


**Figure 2.** Schematic diagram of CMT.

The input or output waves of the resonator are represented by  $B_{\pm}^{in/out}$ ,  $D_{\pm}^{in/out}$ , respectively, and we can obtain:

$$\begin{pmatrix} \gamma_B & -i\mu_1 \\ -i\mu_2 & \gamma_D \end{pmatrix} \cdot \begin{pmatrix} b \\ d \end{pmatrix} = \begin{pmatrix} -\gamma_{OB}^{1/2} & 0 \\ 0 & -\gamma_{OD}^{1/2} \end{pmatrix} \cdot \begin{pmatrix} B_+^{in} + B_-^{in} \\ D_+^{in} + D_-^{in} \end{pmatrix} \quad (5)$$

where  $\mu_1$  and  $\mu_2$  are the coupling coefficients between the bright mode and the dark mode, and their values are equal.

$\gamma_{B(D)}$  is the total loss coefficient,  $\gamma_{iB(D)}$  is the internal loss coefficient, and  $\gamma_{OB(D)}$  is the external loss coefficient.

According to the conservation of energy, the input and output of the bright mode and the dark mode can be expressed as:

$$\begin{cases} D_+^{in} = B_+^{out} e^{i\varphi}, B_-^{in} = D_-^{out} e^{i\varphi} \\ B_{\pm}^{out} = B_{\pm}^{in} - \gamma_{OB}^{1/2} b, D_{\pm}^{out} = D_{\pm}^{in} - \gamma_{OD}^{1/2} d \end{cases} \quad (6)$$

Here, we obtain  $D_-^{in} = 0$  and  $\varphi$  refers to the phase difference between  $b$  and  $d$ . Based on the law of conservation of energy, the results can be seen as:

$$\begin{cases} D_+^{in} = (B_+^{in} - \gamma_{OB}^{1/2} b) e^{i\varphi}, B_-^{in} = -\gamma_{OD}^{1/2} d e^{i\varphi}, \\ D_{\pm}^{out} = (B_{\pm}^{in} - \gamma_{OB}^{1/2} b) e^{i\varphi} - \gamma_{OD}^{1/2} d. \end{cases} \quad (7)$$

Here, with  $\omega_n$  being the  $n$ th resonant angular frequency, the coefficients  $X_{B(D)}$ ,  $\gamma_{B(D)}$  are as follows:

$$\begin{cases} X_{B(D)} = i\mu_{1(2)} + (\gamma_{OB}^{1/2} \gamma_{OD}^{1/2}) e^{i\varphi} \\ \gamma_{B(D)} = i\omega - i\omega_{1(2)} - \gamma_{iB(D)} - \gamma_{OB(D)} \end{cases} \quad (8)$$

The transmission coefficient is obtained by:

$$\begin{aligned} t = \frac{D_+^{out}}{B_+^{in}} &= \frac{B_+^{in} e^{i\varphi} - b e^{i\varphi} \gamma_{OB}^{1/2} - d \gamma_{OD}^{1/2}}{B_+^{in}} = e^{i\varphi} - \frac{b e^{i\varphi} \gamma_{OB}^{1/2} + d \gamma_{OD}^{1/2}}{B_+^{in}} \\ &= e^{i\varphi} - \frac{X_B \gamma_{OB}^{1/2} \gamma_{OD}^{1/2} e^{2i\varphi} + \gamma_D \gamma_{OB} e^{i\varphi} + \gamma_B \gamma_{OD} e^{i\varphi} + X_D \gamma_{OB}^{1/2} \gamma_{OD}^{1/2}}{X_B X_D - \gamma_B \gamma_D} \end{aligned} \quad (9)$$

Thus, the transmittance can be calculated as  $T = |t|^2$ , in which the total loss coefficient, the internal loss coefficient and the external loss coefficient can be calculated by the values of the total quality factors  $Q_{iD}$ , the internal quality factors  $Q_{iB}$ , and the external loss quality factor  $Q_{OB}$  [29]

$$\begin{cases} \gamma_{iB} = \frac{\omega_B}{2Q_{iB}}, \gamma_{iD} = \frac{\omega_D}{2Q_{iD}}, \gamma_{oB} = \frac{\omega_B}{2Q_{oB}}, \gamma_{oD} = \frac{\omega_D}{2Q_{oD}} \\ \frac{1}{Q_{iB}} = \frac{1}{Q_{iB}} + \frac{1}{Q_{oB}}, \frac{1}{Q_{iD}} = \frac{1}{Q_{iD}} + \frac{1}{Q_{oD}} \\ Q_{iB} = \frac{\text{Re}(n_{\text{effB}})}{\text{Im}(n_{\text{effB}})}, Q_{iD} = \frac{\text{Re}(n_{\text{effD}})}{\text{Im}(n_{\text{effD}})} \\ Q_{tB} = \frac{f_B}{\Delta f_B}, Q_{tD} = \frac{f_D}{\Delta f_D} \end{cases} \quad (10)$$

Here, the effective refractive index  $n_{\text{eff}}$  is defined as  $n_{\text{eff}} = \beta/k_0$ . In this work, the direct coupling coefficients between the adjacent modes are uniformly set as  $1.20 \times 10^{11} \text{ rad s}^{-1}$ .  $\varphi$  is the phase shift between the optical bright mode and the optical dark mode, and thus its value is equal to 0 [30].

The definition  $Q_i = \text{Re}(n_{\text{eff}})/\text{Im}(n_{\text{eff}})$  is suitable for resonators made of transmission-line segments. However, only the resistance (ohmic loss) is considered in this definition and the radiation loss is excluded. In addition, there is a similar definition of the total quality factor expressed as  $Q = \text{Re}(\omega)/2\text{Im}(\omega)$  [31], which describes the total factor (including non-radiation and radiation loss). It is suitable for any type of resonant structure.

### 3. Simulation results and applications

Figures 3(a)–(d) show the simulation results. The PIT window at 3.49 THz is achieved in the transmission spectrum, as shown in figure 3(a). To understand the physical mechanism of the PIT effect, one should analyze the contribution of each graphene-metamaterial part of the structure. Thus, the corresponding transmission spectra is illustrated in figure 3(a).

The green line in figure 3(a) shows the bright mode activated by the graphene rectangular cavity and the double outside graphene strips (DOGSs) that can be excited directly by the incident light, as shown by the black line. Additionally, the graphene strip inside the rectangular cavity acts as the dark mode. The inside graphene strip (IGS) cannot interact with the incident wave directly, but can interact with the local field attributed to the coupling of the bright mode and the  $x$ -polarized planar wave. Obviously, the dark mode and the bright mode have flat and narrow spectral lines, respectively. The coupling occurs between the two modes, resulting in a PIT window, just as shown with the red line.

Figures 3(b)–(d) show the distributions of the electric fields corresponding to the points ‘a’, ‘b’ and ‘c’, respectively. As can be seen from figure 3(b), when there is only the DOGSs structure generating the bright mode, the electric field energy is mainly concentrated in the gaps between the graphene rectangular cavity and the double graphene strips. The electric field indicates that the bright mode can be directly excited by the incident light. Meanwhile, from figure 3(c), when there is only the IGS structure, the electric field energy of the dark mode is one order of magnitude smaller than that of the bright mode. The graphene strip is almost not excited so there is less light field localized on it. This shows that the dark mode cannot interact with the incident light directly. As clearly shown in the

transmission spectra, the transmittance is 1.0. For the whole structure in figure 3(d), we can clearly see that the energy of the electric field is limited at the edge of the IGS. This proves that the electric field energy is transferred from the DOGSs structure to the IGS structure, as a result of the near-field coupling between the bright and dark modes. Finally, a distinct transparency window is achieved due to the destructive interference at the frequency of 3.49 THz.

The FDTD simulation is plotted in figures 4(a)–(d). As can be seen from figures 4(a)–(d), the transmission spectrum appears as an approximately linear blue shift, with the increasing Fermi level. This means that the transparent windows can be dynamically modulated by adjusting the bias voltage.

The relationship between voltage and Fermi energy is as follows [32–34]:

$$E_f = \hbar v_F \left( \frac{\pi \varepsilon_0 \varepsilon_d V_g}{d_{\text{sub}} e} \right)^{1/2} \quad (11)$$

where  $V_g$  is the gate voltage,  $v_F$  represents the Fermi carrier velocity, the relative permittivity of air and silica are respectively denoted as  $\varepsilon_0$  and  $\varepsilon_d$ , and  $d_{\text{sub}}$  is the thickness of silica, respectively.

The red dotted lines in figures 4(a)–(d) represent the calculation results by using the CMT theory. The CMT is successfully applied to explain the coupling effect between multiple resonators directly or multiple resonant modes of a single resonator. Here, the FDTD and the CMT results agree with each other, which means that the theoretical model derived from the CMT theory is reasonable for this structure. In addition, a rigorous CMT has been developed for handling graphene-based resonant structures and other nonlinear structures (besides linear ones). Both bulk and sheet nonlinear materials can be allowed by introducing a nonlinear current term into the CMT formulation [35].

In fact,  $Q$  is a measure of the resonant circuit loss. Low loss means a high  $Q$ . The imaginary part of the effective index represents the absorption of electromagnetic waves by a medium. It can be seen from the figures 5(a) and (b) that the real part  $\text{Re}(n_{\text{eff}})$  and the imaginary part  $\text{Im}(n_{\text{eff}})$  of the effective index ( $n_{\text{eff}}$ ) increase with increasing frequency at different Fermi levels. For the graphene layer, with the increase in the working frequency,  $\text{Re}(n_{\text{eff}})$  and  $\text{Im}(n_{\text{eff}})$  increase, but the increase of  $\text{Im}(n_{\text{eff}})$  is much faster at the low frequency.

The values of  $\text{Re}(n_{\text{eff}})$  and  $\text{Im}(n_{\text{eff}})$  at different Fermi levels are shown in figures 5(a) and (b). The values are classified as follows:  $Q_{iB} = (29.9349, 40.3774, 52.5536, 66.3384)$ ,  $Q_{iD} = (32.306, 43.112, 55.4191, 69.202)$ ,  $Q_{oB} = (66.53158, 38.61433, 32.19967, 27.84469)$  and  $Q_{oD} = (54.13636, 38.24202, 30.67984, 27.0987)$  at Fermi levels = (1.1 eV, 1.3 eV, 1.5 eV, 1.7 eV), respectively.

The modulation depth of amplitude (MDA), which is used to describe the capability of the optical switch, can be obtained by [36]:

$$\text{MDA} = \frac{|A_{\text{on}} - A_{\text{off}}|}{A_{\text{on}}} \times 100\%. \quad (12)$$

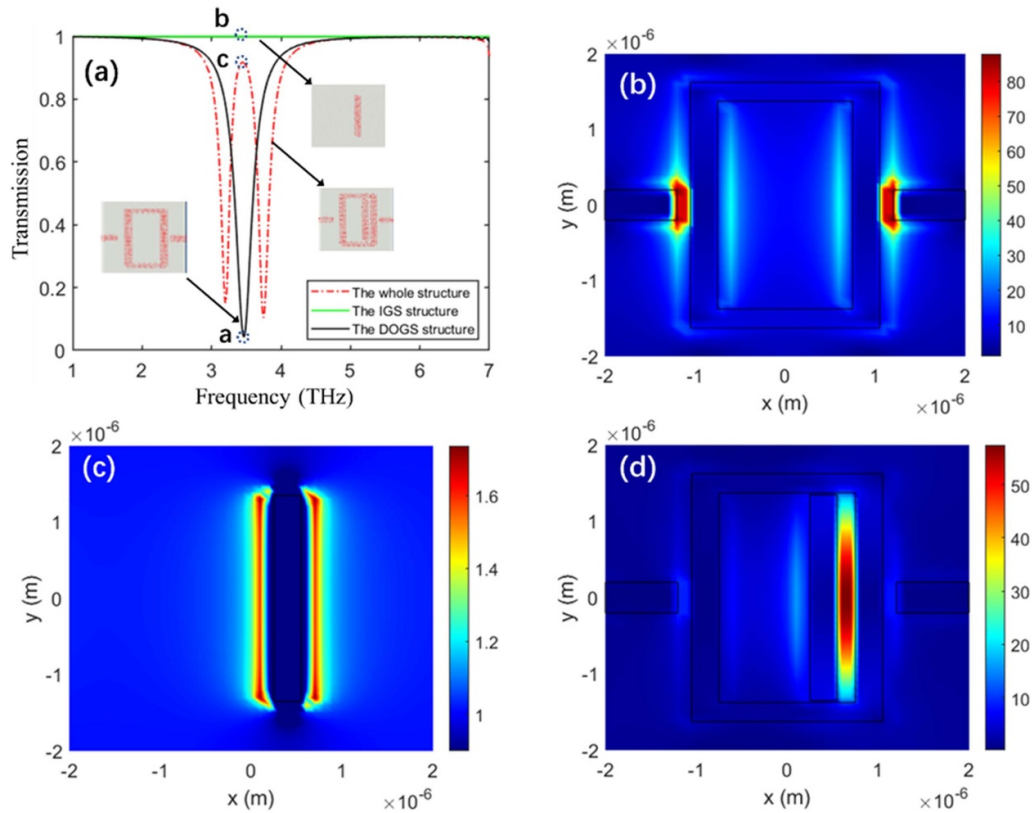


**Figure 3.** (a) Transmission spectra of the graphene structure. (b)–(d) Distributions of the electric field for the corresponding points ‘a’, ‘b’, and ‘c’ at 3.49 THz, here, the Fermi level is set to 1.2 eV.

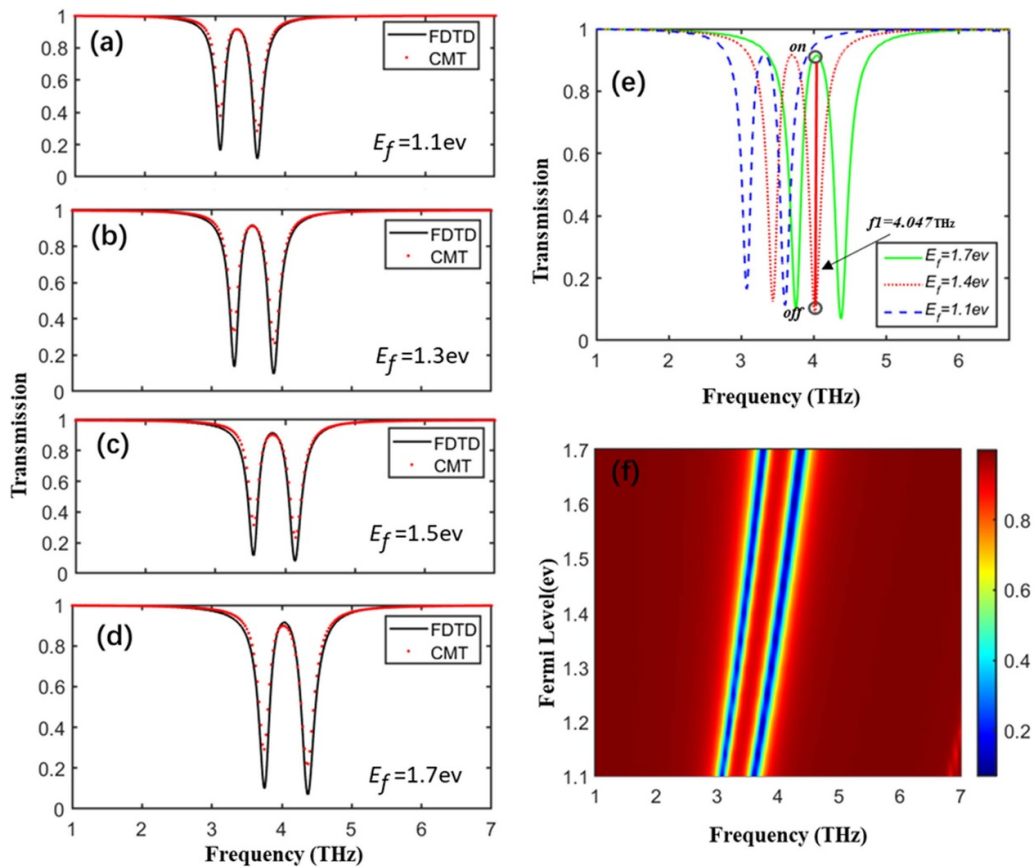


**Figure 4.** (a)–(d) Transmission spectra obtained by FDTD simulation and CMT calculation at different Fermi levels. (e) Modulation mechanism of electro-optical switch. (f) Three-dimensional evolution of the PIT at different Fermi levels.

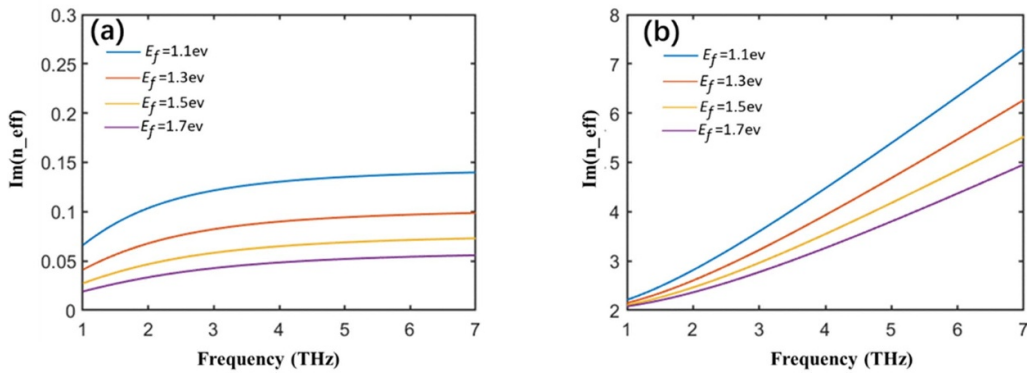


Figure 5. (a), (b) The values of  $\text{Re}(n_{\text{eff}})$  and  $\text{Im}(n_{\text{eff}})$  at different Fermi levels.

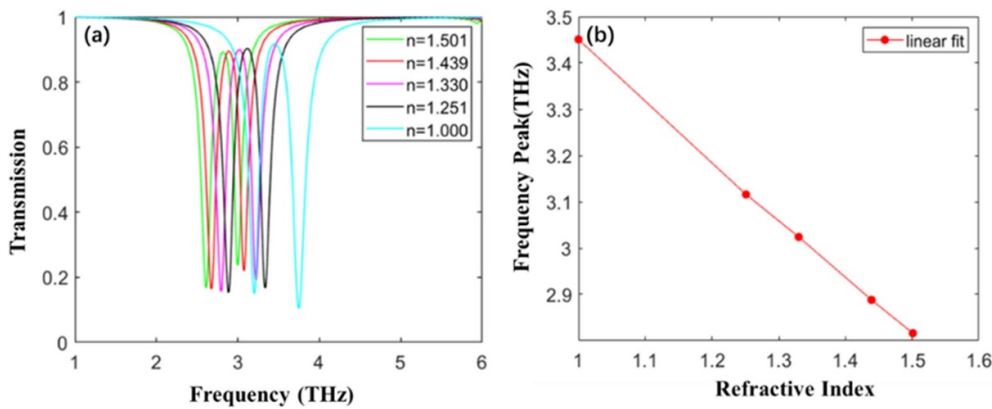


Figure 6. (a) Transmission spectra of the graphene-based PIT structure at different refractive indices, where the Fermi levels is set to 1.2 eV. (b) Relation between resonant PIT peak and refractive index.

According to figure 4(e), the MDA can be calculated as 90.4% at 4.047 THz, and therefore the function of an optical switch can be realized.

Furthermore, the three-dimensional (3D) evolution of the PIT is plotted in figure 4(f), with different Fermi levels. The places where the electric fields are the weakest represent the positions of the two valleys of the transmission spectrum. With the increase in the Fermi level, the positions of the two valleys move from the low frequency to the high frequency and the blue shift of the spectrum is obvious. Such a blue shift can be well understood through the following relationship:  $f_r \propto \sqrt{E_f}$  [34], where  $f_r$  is the resonant frequency.

Different structures which perform as the dark and bright resonators are used to generate the PIT in planar metamaterials [36]. However, in our proposed device, the Fermi level of the graphene material, instead of structural parameters, is used to control the conductivity and adjust the PIT dynamically. This has great advantages in practical applications without changing the geometric size of the structure.

The transmission spectra of air ( $n = 1.000$ ), perfluorohexane ( $n = 1.251$ ), water ( $n = 1.330$ ), 60% glucose solution ( $n = 1.439$ ) and benzene ( $n = 1.501$ ) [5] are also compared. It is obviously observed in figure 6(a) that the transmission spectrum appears to be red-shifted as the refractive index of the surrounding medium increases. Figure 6(a) shows the simulated

PIT spectra with different refractive index at room temperature. The frequencies of the transparent windows decrease linearly with the refractive index of the medium in figure 6(b), and the sensitivity is calculated by the following formula [37, 38]:

$$S = \frac{\Delta f}{\Delta n}. \quad (13)$$

According to equation (13), the sensitivity can be calculated as  $1.335 \text{ THz RIU}^{-1}$ , which means that the structure can be used as a sensor in the terahertz region.

The value of sensitivity exceeded those reported for similar PIT-like graphene metamaterial sensors in the terahertz range [37–39], as shown in table 1. Compared with the sensitivities of other graphene-based sensors, our proposed structure has better sensing performance.

In addition, the influence range of the incident source of the polarization angle ranging from  $0^\circ$  to  $90^\circ$  on the transparent windows is extensively studied, as shown in figures 6(a)–(d). The Fermi level is set to 1.2 eV. Obviously, when the optical polarization angle of the incident light is set as  $0^\circ$ , the PIT window appears at 3.49 THz. While the angle of polarization increases, the PIT window clearly changes.

It can be seen from the transmission spectrum that the points ‘a1’ and ‘a2’ show weakened resonance with the

**Table 1.** Comparison of sensor effects reported with recent studies.

	Our proposed	Reference [37]	Reference [38]	Reference [39]
Sensitivity (THz RIU <sup>-1</sup> )	1.335	1.19	1.18	0.8

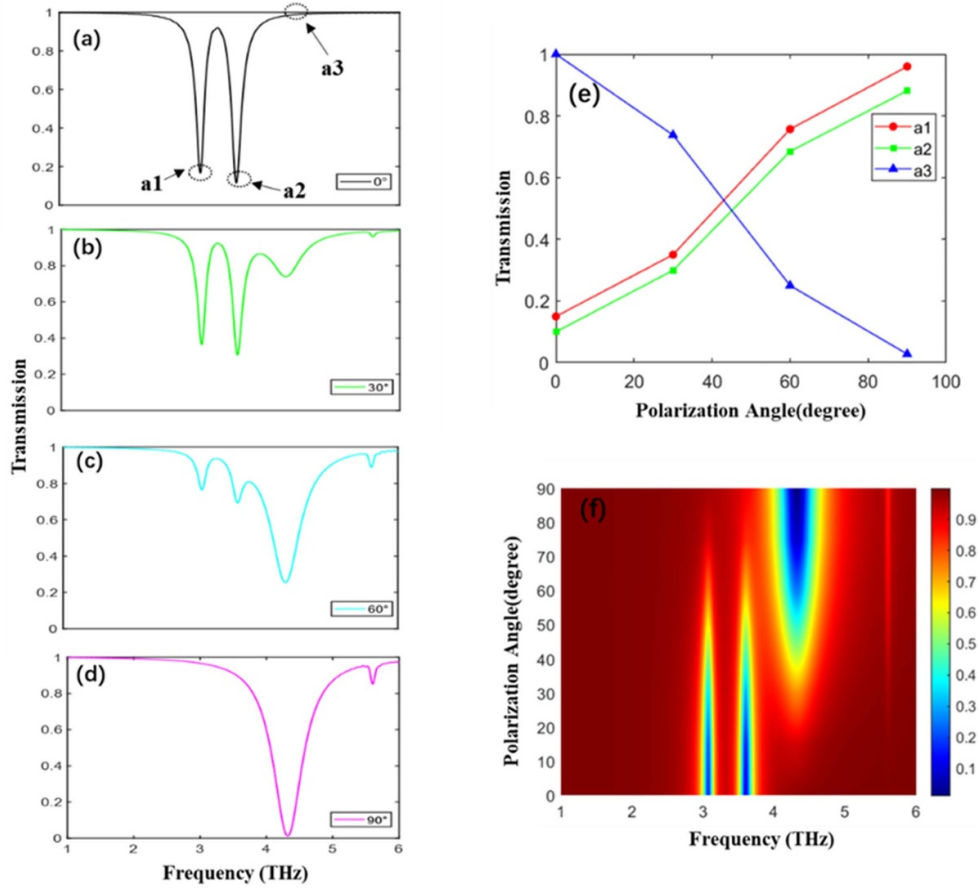


**Figure 7.** (a)–(d) Transmission spectra of the proposed graphene metamaterials with different polarization angle, where the Fermi level is set to 1.2 eV. (e) Transmission shift at points ‘a1’, ‘a2’ and ‘a3’ with polarization angle. (f) Three-dimensional evolution of the polarization angle.

increase of polarization angle in figure 7(e). When the polarization angle is close to 90°, the first and second resonance dips almost disappear. However, in figure 7(e), the third resonance peak appears and the intensity of points ‘a3’ gradually becomes stronger with the increase of the polarization angle. The 3D evolution of the PIT is plotted in figure 7(f). The positions of the three resonant dip angles remain the same independent of the changed polarization angle.

The polarization extinction ratio (PER) is a significant parameter to describe the performance of the polarizer and is calculated by the following formula [40]:

$$PER = 10 \log_{10} \frac{T_{max}}{T_{min}} \text{ (dB)} \quad (14)$$

where,  $T_{max}$ ,  $T_{min}$  represent the transmission amplitudes of ‘on’ and ‘off’ states.

When the polarization angle of incident light reaches 90°, the PERs are 7.60 dB, 8.72 dB and 19.06 dB corresponding to 3.066 THz, 3.606 THz and 4.327 THz. In this case, the Fermi

level is set to 1.2 eV and the environment temperature is a constant value of 300 K. The structural parameters of the proposed periodic metamaterial are shown in figure 1(b).

The PIT is greatly affected by the polarization angle of the incident light and the optical resonance can be controlled. The spectrum with adjustable polarization angle can be obtained directly by the non-contact method, and the tunable polarizer is realized. Compared with previous studies [40, 41], the PIT is more sensitive to the change of the angle of polarization.

#### 4. Conclusion

In summary, the tunable PIT effect has been investigated based on graphene metamaterials. The optical switching function with an amplitude modulation depth of 90.4% is realized by modulating the Fermi energy level of graphene. In addition, the transmission spectra in different surrounding space media have been investigated. We show that the transmission spectrum linearly blue shifts with increasing refractive

index, leading to an index sensitivity of  $1.335 \text{ THz RIU}^{-1}$ . Finally, the dynamic and controllable PIT effects are realized by changing the polarization angle instead of manipulating the structural parameters. Thus, this work lays the foundation for designing chip-scale devices for optical switching and refractive index sensors.

### Data availability statement

All data that support the findings of this study are included within the article (and any supplementary files).

### Acknowledgments

This work was supported by the National Key R&D Program of China (2019YFB1803505); the National Natural Science Foundation of China (62175039, U2001601, 61925501); the Science and Technology Project of Guangzhou (201904010243); Major Special Projects in Guangdong Province (2018B010114002); the Program for Guangdong Introducing Innovative and Entrepreneurial Teams.

### ORCID iDs

Shuxian Chen  <https://orcid.org/0000-0001-9557-5605>

Li Chen  <https://orcid.org/0000-0002-6587-0272>

Kunhua Wen  <https://orcid.org/0000-0002-7658-8731>

### References

- [1] Chen F, Zhang H, Sun L and Yu C 2019 *Optik* **196** 163139
- [2] Zhang J, Zhang L and Xu W 2012 *J. Phys. D: Appl. Phys.* **45** 113001
- [3] Xu H, Xiong C, Chen Z, Zheng M, Zhao M, Zhang B and Li H 2018 *J. Opt. Soc. Am. B* **35** 1463–8
- [4] Gao W, Shi G, Jin Z, Shu J, Zhang Q, Vajtai R, Ajayan P M, Kono J and Xu Q 2013 *Nano Lett.* **13** 3698–702
- [5] Gao W, Shu J, Qiu C and Xu Q 2012 *ACS Nano* **6** 7806–13
- [6] Liu Z, Gao E, Zhang X, Li H, Xu H, Zhang Z, Luo X and Zhou F 2020 *New J. Phys.* **22** 053039
- [7] Farmani A, Mir A and Sharifpour Z 2018 *Appl. Surf. Sci.* **453** 358–64
- [8] Fu G-L, Zhai X, Li H-J, Xia S-X and Wang L-L 2016 *J. Opt.* **19** 015001
- [9] Vakili A and Engheta N 2011 *Science* **332** 1291–4
- [10] Zhang S, Genov D A, Wang Y, Liu M and Zhang X 2008 *Phys. Rev. Lett.* **101** 047401
- [11] Ketzaki D A, Tsilipakos O, Yioultsis T V and Kriezis E E 2013 *J. Appl. Phys.* **114** 113107
- [12] Grebenchukov A, Masyukov M, Zaitsev A and Khodzitsky M 2020 *Opt. Commun.* **476** 126299
- [13] Ono M, Hata M, Tsunekawa M, Nozaki K, Sumikura H, Chiba H and Notomi M 2020 *Nat. Photon.* **14** 37–43
- [14] Wang R, Ren X-G, Yan Z, Jiang L-J, Sha W and Shan G-C 2019 *Front. Phys.* **14** 1–20
- [15] Xiong C X, Chao L, Zeng B, Wu K, Li M, Ruan B X, Zhang B H, Gao E D and Li H J 2021 *Phys. Chem. Chem. Phys.* **23** 3949–62
- [16] Guan J, Xia S, Zhang Z, Wu J, Meng H, Yue J, Zhai X, Wang L and Wen S 2020 *Nanoscale Res. Lett.* **15** 1–13
- [17] Chou Chau Y-F, Chou Chao C-T, Huang H J, Kooch M R R, Kumara N T R N, Lim C M and Chiang H-P 2020 *Nanomaterials* **10** 2030
- [18] Cheng H, Chen S, Yu P, Duan X, Xie B and Tian J 2013 *Appl. Phys. Lett.* **103** 203112
- [19] Li H, Ji C, Ren Y, Hu J, Qin M and Wang L 2019 *Carbon* **141** 481–7
- [20] He X, Zhong X, Lin F and Shi W 2016 *Opt. Mater. Express* **6** 331–42
- [21] He X 2015 *Carbon* **82** 229–37
- [22] Andryeuskii A and Lavrinenko A V 2013 *Opt. Express* **21** 9144–55
- [23] Ju L, Geng B, Horng J, Girit C, Martin M, Hao Z, Bechtel H A, Liang X, Zettl A and Shen Y R 2011 *Nat. Nanotechnol.* **6** 630–4
- [24] Han X, Wang T, Li X, Xiao S and Zhu Y 2015 *Opt. Express* **23** 31945–55
- [25] Sun D, Wu Z K, Divin C, Li X, Berger C, de Heer W A, First P N and Norris T B 2008 *Phys. Rev. Lett.* **101** 157402
- [26] Haus H A and Huang W 1991 *Proc. IEEE* **79** 1505–18
- [27] Tsakmakidis K L, Shen L, Schulz S A, Zheng X, Upham J, Deng X, Altug H, Vakakis A F and Boyd R W 2017 *Science* **356** 1260–4
- [28] Liu Z M, Gao E D, Zhang Z B, Li H J, Xu H, Zhang X, Luo X and Zhou F Q 2020 *Nanoscale Res. Lett.* **15** 1–9
- [29] Lu H, Liu X and Mao D 2012 *Phys. Rev. A* **85** 053803
- [30] Xiong C, Xu H, Zhao M, Zhang B, Liu C, Zeng B, Wu K, Ruan B, Li M and Li H 2021 *Sci. China Phys. Mech. Astron.* **64** 224211
- [31] Chen Y-L, Zou C-L, Hu Y-W and Gong Q 2013 *Phys. Rev. A* **87** 023824
- [32] Fei Z, Rodin A, Andreev G O, Bao W, Mcleod A, Wagner M, Zhang L, Zhao Z, Thiemens M and Dominguez G 2012 *Nature* **487** 82–85
- [33] Wang Y, Cui W, Ma H, Xu H, Yi Z, Cao X, Ren X and He Z 2021 *Results Phys.* **23** 104002
- [34] Jiang J, Zhang Q, Ma Q, Yan S, Wu F and He X 2015 *Opt. Mater. Express* **5** 1962–71
- [35] Christopoulos T, Tsilipakos O, Grivas N and Kriezis E E 2016 *Phys. Rev. E* **94** 062219
- [36] Tassin P, Zhang L, Koschny T, Economou E and Soukoulis C M 2009 *Opt. Express* **17** 5595–605
- [37] Fan C, Ren P, Jia W, Jia Y and Wang J 2019 *Superlattices Microstruct.* **136** 106295
- [38] Wang K, Fan W-H, Chen X, Song C and Jiang X-Q 2019 *Opt. Commun.* **439** 61–65
- [39] Jiang W and Chen T 2021 *Diam. Relat. Mater.* **118** 108531
- [40] Zhang X, Liu Z, Zhang Z, Gao E, Luo X, Zhou F, Li H and Yi Z 2020 *Opt. Express* **28** 36771–83
- [41] Ren P, Jia Y and Fan C 2020 *J. Phys. Chem. C* **124** 21075–81